AGU PUBLICATIONS

Water Resources Research

RESEARCH ARTICLE

10.1002/2015WR017098

# Water table salinization due to seawater intrusion

**Sugiarto Badaruddin[1,2,3], Adrian D. Werner[1,2], and Leanne K. Morgan[1,2]**

[1]National Centre for Groundwater Research and Training, Flinders University, Adelaide, South Australia, Australia, [2]School of the Environment, Flinders University, Adelaide, South Australia, Australia, [3]Civil Engineering Department, State Polytechnic of Ujung Pandang, South Sulawesi, Indonesia

**Key Points:**
- Physical experiments of seawater intrusion and WTS reproduced in numerical model
- Field-scale models show temporarily faster WTS than interface toe movements
- Largest WTS produced by aggressive seawater intrusion in deep, high conductivity aquifers

**Correspondence to:**
S. Badaruddin,
sugi0040@flinders.edu.au

**Citation:**
Badaruddin, S., A. D. Werner, and L. K. Morgan (2015), Water table salinization due to seawater intrusion, *Water Resour. Res.*, *51*, 8397–8408, doi:10.1002/2015WR017098.

Received 18 FEB 2015
Accepted 27 SEP 2015
Accepted article online 1 OCT 2015
Published online 23 OCT 2015

**Abstract** Seawater intrusion (SWI) is a significant threat to freshwater resources in coastal aquifers around the world. Previous studies have focused on SWI impacts involving salinization of the lower domain of coastal aquifers. However, under certain conditions, SWI may cause salinization of the entire saturated zone of the aquifer, leading to water table salinization (WTS) in unconfined aquifers by replacing freshwater within the upper region of the saturated zone with seawater, thereby posing a salinity threat to the overlying soil zone. There is presently limited guidance on the extent to which WTS may occur as a secondary impact of SWI. In this study, physical experiments and numerical modeling were used to explore WTS associated with SWI in various nontidal, unconfined coastal aquifer settings. Laboratory experiments and corresponding numerical simulations show that significant WTS can occur under active SWI (i.e., the freshwater hydraulic gradient slopes toward the land) because the cessation of freshwater discharge to the sea and the subsequent landward flow across the entire sea boundary eventually lead to water table salinities approaching seawater concentration. WTS during active SWI is larger under conditions of high hydraulic conductivity, rapid SWI, high dispersivity and for deeper aquifers. Numerical modeling of four published field cases demonstrates that rates of WTS of up to 60 m/yr are plausible. Under passive SWI (i.e., the hydraulic gradient slopes toward the sea), minor WTS may arise as a result of dispersive processes under certain conditions (i.e., high dispersivity and hydraulic conductivity, and low freshwater discharge). Our results show that WTS is probably widespread in coastal aquifers experiencing considerable groundwater decline sustained over several years, although further evidence is needed to identify WTS under field settings.

## 1. Introduction

Currently, coastal aquifers worldwide are under increasing threat of seawater intrusion (SWI) [*Ferguson and Gleeson*, 2012; *Werner et al*., 2013]. SWI is a phenomenon where seawater encroaches into a coastal aquifer and contaminates fresh groundwater [*Bear*, 1979]. The occurrence of SWI is most commonly associated with the penetration of seawater within the lower domain of a coastal aquifer, due to the higher density of seawater relative to the ambient groundwater. However, *Werner and Lockington* [2006] identified the potential for SWI to induce water table salinization (WTS) within unconfined aquifer settings. This occurs when SWI causes salinization of the entire saturated profile of the aquifer, leading to saline water occurring at the water table of unconfined coastal aquifers. *Werner and Lockington* [2006] focused on the effects of tides and rapid decline in the water table elevation as important factors leading to WTS, although their investigation of WTS was limited to a single situation involving estuarine SWI. The occurrence of WTS may have significant implications for unsaturated zone water quality and productivity, since WTS may lead to soil salinization [*Prathapar et al*., 1992; *Werner and Lockington*, 2004, 2006; *Ibrahimi et al*., 2014]. WTS due to SWI has not been documented in real-world settings or under controlled laboratory situations, and hence the occurrence, extent and causes of WTS remain unclear.

In this study, physical experiments and numerical modeling are combined to examine the occurrence of WTS associated with SWI in response to an inland freshwater head drop. Comparing the laboratory and numerical modeling results offers insight into both the veracity of the laboratory setup and the assumptions of the numerical code. WTS is examined in the absence of tidal effects, and the analysis focuses on the influence of water table decline on WTS. We anticipate that more aggressive SWI will lead to WTS, in accordance with *Werner and Lockington*'s [2006] prediction of WTS during rapid water table decline. The effects of freshwater head declines (rather than sea level rise) on WTS are considered in this study, because these are expected to develop faster and be larger in magnitude than sea level rise, and are therefore more likely to generate more aggressive SWI situations [*Intergovernmental Panel on Climate Change*, 2008; *Werner et al*., 2013].

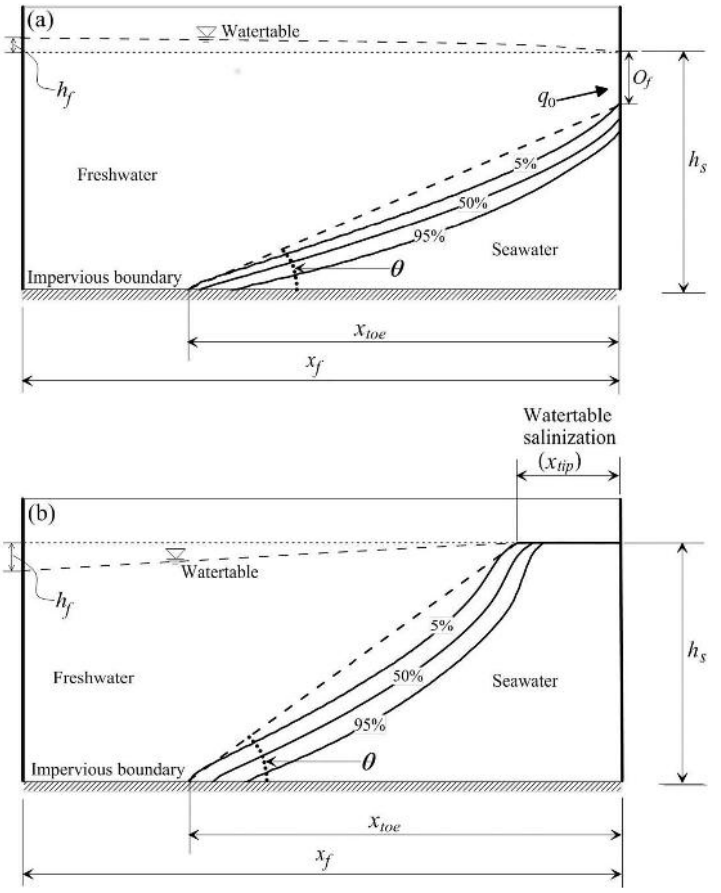


**Figure 1.** Conceptual schematic of (a) passive SWI and (b) active SWI. $h_f$ is the height of the water table at the inland boundary measured from sea level and is negative for active SWI cases, $x_f$ is the distance to the inland boundary condition [$L$], and $h_s$ is the depth of the horizontal base of the aquifer below sea level [$L$].

## 2. WTS Conceptual Models: Active and Passive SWI

Previous studies identify two different modes of SWI: passive and active [*Bear and Dagan*, 1964; *Mahesha*, 1995; *Werner et al.*, 2012]. In the former, SWI occurs despite persistent freshwater discharge to the sea, and the seawater wedge intrudes rather slowly. Where passive SWI arises from a reduction in the water table elevation, there will be an accompanying decrease in the depth of freshwater discharging at the shoreline [*Werner et al.*, 2012; *Morgan et al.*, 2012], referred to here as the freshwater outflow face ($O_f$ [$L$]) as shown in Figure 1a. Where the discharge face is not vertical, there will nonetheless be a depth of freshwater discharge at the shoreline that separates seawater from the water table (in the absence of tidal effects) [*Bakker*, 2006; *Benson et al.*, 1998]. It is hypothesized that, in the case of nontidal passive SWI, there may be an increase in water table salinities accompanying a reduction in $O_f$, largely due to dispersive effects and the closer proximity of the seawater wedge to the water table. Here we define WTS as the distance from the shoreline to the "tip" of the seawater wedge ($x_{tip}$ [$L$]; Figure 1b), which is designated by a particular salinity. The seawater wedge "toe" is the extent of seawater along the aquifer basement ($x_{toe}$ [$L$]; Figure 1). Following *Mehdizadeh et al.* [2014], $x_{tip}$ and $x_{toe}$ are calculated using 5% of seawater salinity. By connecting the toe and the tip of the interface with a straight line, the interface alignment ($\theta$) is defined as shown in Figures 1a and 1b.

In the limiting condition where freshwater discharge to the sea ($q_0$ [$L^2/T$]) ceases, a transition occurs from passive SWI to active SWI at the shoreline. The cessation of $q_0$ reduces $O_f$ to zero, which causes the freshwater-saltwater interface tip to occur at, rather than below, the water table. Active SWI is driven by the combined effects of the density difference between freshwater and seawater, and the inland-sloping hydraulic gradient, whereas in passive SWI, these forces are opposed. We expect significantly more extensive WTS under active SWI. The rate of WTS under both active and passive SWI is likely to be a nonlinear function of several parameters given the complex nature of the density-dependent flow and transport relationships accompanying transient SWI [*Lu and Werner*, 2013].

## 3. Experimental Methods and Materials

### 3.1. Laboratory Experiments

Laboratory experiments were undertaken using the same apparatus as that used by *Mehdizadeh et al.* [2014]. The sand tank has internal dimensions of 117.0 cm (length), 5.2 cm (width), and 60.0 cm (height) and is constructed of 10 mm thick transparent plate glass supported by a stainless steel frame. We

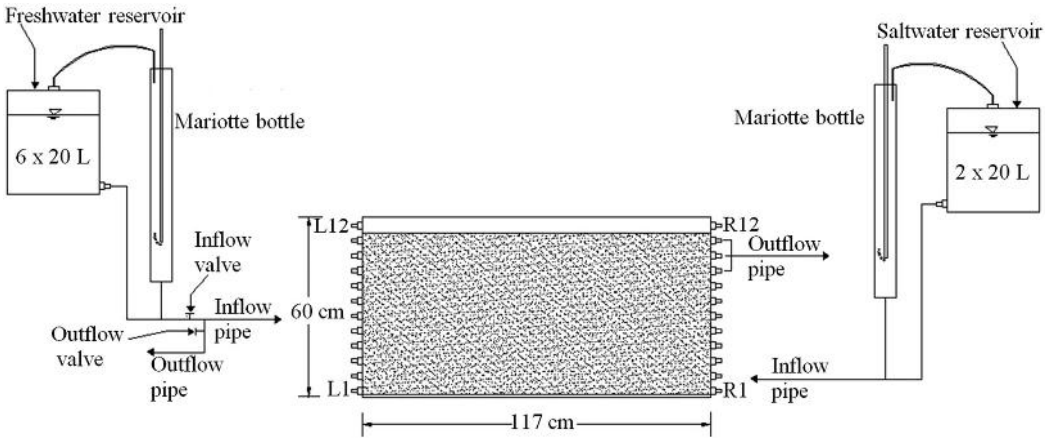


**Figure 2.** Schematic of the sand-tank setup. The inland and seaside boundaries are the left and right sides of the tank, respectively.

acknowledge the small scale of the sand tank, relative to real-world conditions, as a limitation of the laboratory experiments. However, there is a lack of field-based investigations of WTS, and hence, these are the only nonmodeling observations of this phenomenon that are presently available. The tank was filled with sand to a height of 52.0 cm. Twelve plastic inflow and outflow ports are installed at 5.0 cm intervals along the sides of the tank. A schematic of the experimental setup is shown in Figure 2.

Head boundaries of the tank (inland and seaside) were controlled using Mariotte bottles connected to the inflow-outflow taps. The water and gas components of the Mariotte bottles were interconnected, following *Klute and Dirksen* [1986]. In steady-state experiments, saltwater entered the tank through taps R2-R7, freshwater entered through taps L2-L11, and taps R9-R11 provided mixed-water discharge (Figure 2). A specified-head condition was applied to the entire right boundary of the sand tank (sea boundary) to represent seawater hydrostatic heads.

The tank arrangement allowed for either inflow or outflow of freshwater through the inland boundary, depending on whether passive or active SWI conditions were being explored. Taps R9-R11 in Figure 2 were closed when the head at the inland boundary dropped lower than the sea boundary in order to prevent mixed water being drawn into the sand tank under active SWI conditions. Three manometers were attached to taps L1, R1, and R8 to monitor the head at both the inland and sea boundaries (see Figure 2).

A saltwater solution was produced using 1400 g of calcium chloride dehydrate ($CaCl_2.2H_2O$) dissolved in 40 L of tap water (freshwater). Following *Werner et al.* [2009], Rhodamine WT (fluorescent FWT Red dye, ENVCO, Australia) with concentration of 500 mg/L was used as a visual tracer of saltwater movement in the tank. Rhodamine WT has been widely and successfully used in sand-tank models previously [e.g., *Schincariol and Schwartz*, 1990; *Werner et al*., 2009; *Jakovovic et al*., 2011*; Shi et al*., 2011; *Jakovovic et al*., 2012]. Saltwater density ($\rho_s$ [$M/L^3$]) and freshwater density ($\rho_f$ [$M/L^3$]) were 1018.3 and 998.1 kg/m$^3$, respectively (determined using a pycnometer and mass-volume measurements), and a saltwater concentration ($C_s$ [$M/L^3$]) of 26.4 kg/m$^3$ was calculated. The saltwater concentration value of 26.4 kg/m$^3$ indicates the total mass of salt per unit volume of water. The density of saltwater used in the physical experiment (1018.3 kg/m$^3$) is relatively low compared to typical seawater density (1025 kg/m$^3$). This increased the amount of time and space available within sand-tank experiments to observe the interface movement under active SWI conditions, before the interface toe reached the inland boundary. SEAWAT modeling indicated that using a lower saltwater density of 1018.3 kg/m$^3$ instead of 1025 kg/m$^3$ increased the physical modeling duration from 10 to 20 min (the results are not shown for brevity). In addition, a lower saltwater density (i.e., 1015.1 kg/m$^3$) has been successfully used previously by *Morgan et al*. [2013c] to explore SWI transient effects in physical experiments. The experiments were recorded using an 8 mega-pixel digital camera and pictures were taken at 15 min intervals for passive SWI experiments and at 0.5 min intervals for active SWI experiments.

Medium-grained sand (i.e., "16–30" grade sands, Sloan Sands P/L, Dry Creek, South Australia) was the porous medium used in the experiments. A wet-packing method was adopted to obtain a relatively uniform level

of compaction and minimal entrapped air [*Ojuri and Ola*, 2010]. Porosity ($n$) of the sand was measured by the water saturation method [*Fetter*, 2001] and found to be 0.41. The sand hydraulic conductivity ($K$ [$L/T$]) was estimated by two different methods: (1) constant head (Darcy column test) and (2) sieve/grain-size analysis combined with the Kozeny-Carman formula [*Freeze and Cherry*, 1979]. Darcy column tests used a 37 cm long, 5 cm internal diameter acrylic cylinder and were conducted three times. The sand was packed under saturated conditions in a similar fashion to the sand-tank experimental setup. The average $K$ obtained from Darcy column tests was 269 m/d. The grain-size distribution curve from the sieve analysis gave values for $d_{10}$, $d_{50}$, and $d_{60}$ of 0.57, 0.64, and 0.78 mm, respectively, and 1.37 for the uniformity coefficient ($d_{60}/d_{10}$). Applying these values to the Kozeny-Carman formula provided a $K$ of 308 m/d. Since the same wet-packing method was adopted in filling both the sand tank and the Darcy column, the value of 269 m/d was used for horizontal and vertical $K$ in the numerical model of laboratory experiments. The saturation and drainage method described by *Johnson* [1967] was used to obtain a specific yield ($S_y$) of 0.32 for the sand.

Prior to commencing the transient experiment, $h_f$ and $h_s$ were maintained at 2.2 and 48.2 cm, respectively (refer to Figure 1), for several hours in order to establish steady-state conditions. Steady-state conditions were confirmed by monitoring both the toe position and the discharge flux for 4 hours, after which time no changes were observed. Passive SWI in response to a freshwater head decline (FHD) was induced by lowering $h_f$ from 2.2 to 1.2 cm instantaneously (refer to Figure 1). After 210 min of passive SWI, the interface toe reached about half of the aquifer length (i.e., 62.0 cm). Numerical modeling indicated that the interface was still moving at this time. Steady-state conditions would require an additional 840 min to reach a stable $x_{toe}$ of 73.3 cm from the sea boundary (the results are not shown for brevity). After 210 min, $h_f$ was instantaneously dropped from 1.2 to −4.8 cm (refer to Figure 1) to induce active SWI. The experiment continued until the wedge almost reached the inland boundary (i.e., after 18 min of active SWI). The position of the toe and the tip of the interface were estimated from visual inspection of the experimental photography, which captured the distribution of the visual tracer. In situ salinity measurements were not possible using the current sand tank, and therefore salt distributions were explored only through a comparison of numerical modeling and visual inspection of physical experiments.

### 3.2. Numerical Model

The variable-density groundwater flow and transport code SEAWAT version 4 [*Langevin et al*., 2008] was used to simulate transient SWI in laboratory experiments and at the field scale. SEAWAT has been validated using several benchmark problems [e.g., *Langevin et al*., 2003; *Brovelli et al*., 2007; *Goswami and Clement*, 2007], and is widely used, and thus the governing equations from the user manual [*Guo and Langevin*, 2002] are not rewritten here for brevity.

The model domain used in the numerical model was in accordance with the dimensions of the sand tank as shown in Figure 2. Dirichlet conditions for head were used to represent the sand-tank side boundaries, and no-flow conditions were assigned to the bottom of the model. In SEAWAT simulations, a specified-head condition was assigned to the vertical coastal boundary to represent the density-dependent head distribution of the ocean [*Langevin et al*., 2008]. The concentration boundary condition at the coastal boundary is one where inflowing water has the concentration of seawater, whereas outflowing water is assigned the ambient concentration of groundwater at the boundary. In this way, inflow causes the coastal boundary cells to approach seawater concentration, and discharge through the boundary generally causes a reduction in the boundary salinity. At the coastal boundary, the equivalent freshwater head remains unchanged throughout the simulation, despite that the solute concentration at the boundary varies depending on the direction of flow. The CHD package of SEAWAT was used to represent the instantaneous inland FHD. Numerical modeling adopted a molecular diffusivity $D_m$ [$L^2/T$] of $10^{-9}$ $m^2/s$, and longitudinal dispersivity $\alpha_L$ [$L$] was 0.4 cm, as derived from the *Ogata and Banks* [1961] analytical solution and breakthrough fitting curves obtained during the Darcy column tests. Following *Abarca et al*. [2004], transverse dispersivity $\alpha_T$ [$L$] was assumed to be one tenth of $\alpha_L$. Discretization of the model domain was initially estimated using the grid Peclet number ($Pe$) criterion [*Voss and Souza*, 1987]:

$$Pe = \frac{q_f \Delta L}{D_m + \alpha_L q_f} \approx \frac{\Delta L}{\alpha_L} \leq 4 \tag{1}$$

where $q_f$ [$L/T$] is the local groundwater velocity and $\Delta L$ [$L$] is the grid spacing. The total height of the porous medium used in the numerical model was 52 cm. A uniform grid size of $\Delta x = 0.50$ cm and $\Delta z = 0.50$ cm

**Table 1.** Parameter Values for SWI Case Studies

| | Case Study | | | |
|---|---|---|---|---|
| Parameter | 1 | 2 | 3 | 4 |
| FHD rate (m/yr) | 0.32 | 0.02 | 0.48 | 0.12 |
| FHD period (years) | 17 | 26 | 13 | 39 |
| $K$ (m/d) | 166 | 10 | 7 | 45 |
| $h_s$ (m) | 37 | 20 | 50 | 120 |
| Initial $h_f$ (m) | 4.64 | 1.12 | 1.30 | 3.40 |
| Post-SWI $h_f$ (m) | −0.80 | 0.60 | −5.00 | −1.43 |
| $x_f$ (m) | 4750 | 1250 | 2000 | 2700 |
| $n$ | 0.10 | 0.30 | 0.27 | 0.30 |
| $S_y$ | 0.05 | 0.20 | 0.20 | 0.25 |
| $\alpha_L$ (m) | 10 | 1 | 10 | 10 |
| $\alpha_T$ (m) | 1 | 0.1 | 1 | 1 |
| $D_m$ ($m^2$/d) | 0 | 0 | 0 | 0 |
| $\delta$ | 0.025 | 0.025 | 0.025 | 0.025 |
| $W_{net}$ (mm/yr) | 110 | 20 | 33 | 15 |

resulted in a grid of 24,336 cells and a *Pe* of 1.25. This discretization scheme was then further validated by comparing the simulation results of a finer grid size with $\Delta x = 0.25$ cm and $\Delta z = 0.50$ cm, and the difference in the interface position was less than 0.05 cm. A time step of 30 s was employed, and the transport step size was set to 3 s. Three stress periods were defined in the numerical model of laboratory experiments, as (1) a 4 h period to reach steady-state conditions with $h_s$ at 48.2 cm and $h_f$ at 2.2 cm (refer to Figure 1), (2) $h_f$ was dropped by 1.0 cm instantaneously, and passive SWI was simulated for 210 min, and (3) $h_f$ was dropped instantaneously by 6.0 cm to produce active SWI for 18 min.

SWI simulations of several simplified field settings, using parameters from published case studies, were undertaken to gain insight into WTS under more realistic conditions relative to laboratory-scale experiments. Following *Jakovovic et al.* [2011] and *Morgan et al.* [2013c], no calibration of the laboratory and field-scale models was undertaken in this study. The SWI case studies and their related parameters are summarized in Table 1. Only brief descriptions are provided for the SWI field cases. The reader is directed to publications by *Werner and Gallagher* [2006], *Kouzana et al.* [2009], *Ayni et al.* [2011], *Cook et al.* [2013], and *Morgan et al.* [2013a,b] for a complete account of the respective field settings. Case 1 parameters apply to the Pioneer Valley unconfined aquifer, Australia [*Werner and Gallagher*, 2006; *Morgan et al.*, 2013a], Case 2 parameters represent the Quaternary unconfined aquifer in Willunga Basin, Australia [*Morgan et al.*, 2013b], Case 3 parameters are based on the Korba aquifer, Tunisia [*Kouzana et al.*, 2009; *Ayni et al.*, 2011], and Case 4 represents the Cape Range Group aquifer, Australia [*Cook et al.*, 2013]. In Table 1, the initial and post-SWI values of $h_f$ were taken from well observations located at a distance ($x_f$ [*L*]) from the coast in each of the study areas. The initial $h_f$ values for Cases 1, 2, 3, and 4 were measured in years 1988, 1988, 1993, and 1955, respectively, and $h_f$ values following water table decline were measured in years 2005, 2014, 2006, and 1994, respectively. $W_{net}$ [*L*/*T*] and $\delta$ in Table 1 are distributed net recharge and dimensionless density ratio $\delta = (\rho_s - \rho_f)/\rho_f$, respectively.

## 4. Results and Discussion

### 4.1. Comparison Between Laboratory Experiments and Numerical Modeling

In this study, the sand-tank experiments focus on validating SEAWAT's use in simulating WTS. We tested SEAWAT's ability to predict WTS because the code considers saturated conditions only, whereas the sand-tank and field settings include both saturated and unsaturated conditions, and our study focuses on the saturated-unsaturated interface. Furthermore, SEAWAT has not been used to investigate WTS previously. The results of the laboratory experiments are presented in Figure 3. The initial steady-state interface is shown in Figure 3a, which indicates a reasonable match between the physical experiment and numerical model. There was also a reasonable match between the physical experiment and numerical model following passive and active SWI conditions as shown in Figure 3b (210 min of passive SWI) and Figure 3c (after 13 min of active SWI), respectively. Sand tank and numerical modeling values of $x_{toe}$, $x_{tip}$, and $\theta$ for the conditions shown in Figure 3 are listed in Table 2.

The sharp interface observed in the laboratory experiment appeared wider in the numerical model under passive SWI conditions, but overall a reasonable match was observed for both steady-state and passive SWI conditions. The interface was highly dispersed and uneven under active SWI in the laboratory experiment (refer to Figure 3c). In the numerical model, the interface was wider during active SWI than in the passive case, in agreement with the laboratory results. However, the irregular shape of the laboratory interface, likely caused by small-scale heterogeneities, was smooth in the numerical model. That is, the high flow velocities associated with active SWI accentuate variability in the shape of the freshwater-saltwater interface due to heterogeneity effects. This process is simulated in an averaged manner by the velocity-dependent

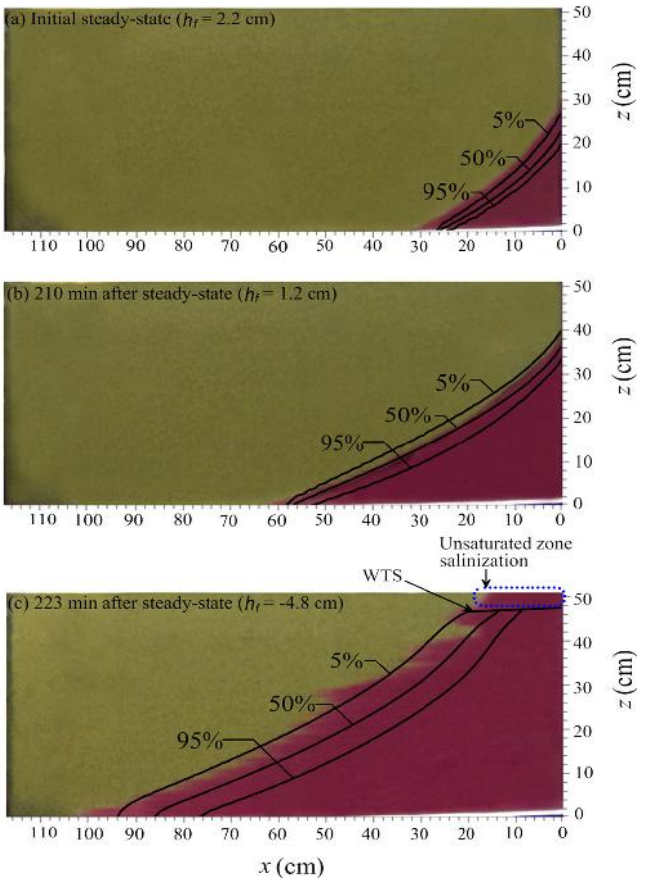


**Figure 3.** Comparison of observed saltwater wedge profiles between physical experiments and numerical modeling for (a) initial steady-state conditions, (b) following 210 min of passive SWI, and (c) after 13 min of active SWI (black lines represent the numerical modeling results).

dispersion of SEAWAT, which reproduces reasonably well the widening of the interface under active SWI conditions.

As shown in Figure 3, a more aggressive landward movement of the interface occurred under active SWI compared to passive SWI, as expected. Active SWI was accompanied by WTS within both the physical experiment and numerical model (Figure 3c). The salinization of the water table led to salinization of the overlying unsaturated zone near the coastal boundary of the laboratory experiment (Figure 3c). The saturation-only approach of SEAWAT cannot simulate this effect. This provides an initial indication, albeit only at the laboratory scale, that unsaturated zone salinization arising from active SWI is a plausible occurrence. *Werner and Lockington* [2004] undertook a simple 1-D numerical investigation of salt rise from salinity-impacted water tables and found that surface salinization was a plausible outcome of enhanced water table salinities due to SWI. However, further investigation of this process is needed to investigate the likely extent of unsaturated zone salinization under field-scale conditions.

Figures 4a, 4b, and 4c show the transient values of $x_{toe}$, $x_{tip}$, and $\theta$, respectively, as obtained from the physical experiments and numerical modeling. $x_{toe}$ increased gradually under passive SWI and then rapidly under active SWI (Figure 4a). $x_{tip}$ was 0.0 cm during passive SWI and increased abruptly following the commencement of active SWI. $\theta$ values decreased with time in both the physical experiments and numerical modeling during passive SWI because the toe of the wedge advanced inland and the tip did not advance landward. The commencement of active SWI via the instantaneous FHD of 6.0 cm (after 210 min) eliminated freshwater discharge $q_0$ to the sea boundary and the accompanying outflow face (i.e., $O_f$ was 8.2 cm in the numerical model and 9.2 cm in the physical experiment) after 1 min. Once the tip of the saltwater wedge reached the water table, $\theta$ increased abruptly in the physical experiment and the numerical model, from 32.2° to 36.8° and 34.4° to 38.1°, respectively, after 1 min of active SWI. This indicates faster inland movement of the interface tip relative to the toe during the initial stages of active SWI in both the physical experiment and the numerical model. $\theta$ subsequently decreased during the rest of simulation. At the conclusion of the experiment (after 228 min), $\theta$ had reduced to 29.5° in the physical experiment and 31.3° in the numerical model, indicating faster toe movement relative to the tip during the later stages of active SWI.

**Table 2.** The Values of $x_{toe}$, $x_{tip}$, and $\theta$ Obtained From Physical Experiments and Numerical Modeling for the Conditions Shown in Figure 3

| | Physical Experiment Time (min) | | | Numerical Model Time (min) | | |
|---|---|---|---|---|---|---|
| Parameter | 0 (Steady State) | 210 | 223 | 0 (Steady State) | 210 | 223 |
| $x_{toe}$ (cm) | 31.9 | 62.0 | 103.1 | 26.2 | 58.4 | 93.8 |
| $x_{tip}$ (cm) | 0.0 | 0.0 | 23.0 | 0.0 | 0.0 | 19.5 |
| $\theta$ (°) | 42.3 | 32.2 | 30.7 | 45.3 | 34.4 | 32.6 |

Particle tracking modeling using PMPATH [*Chiang and Kinzelbach*, 1994] was undertaken

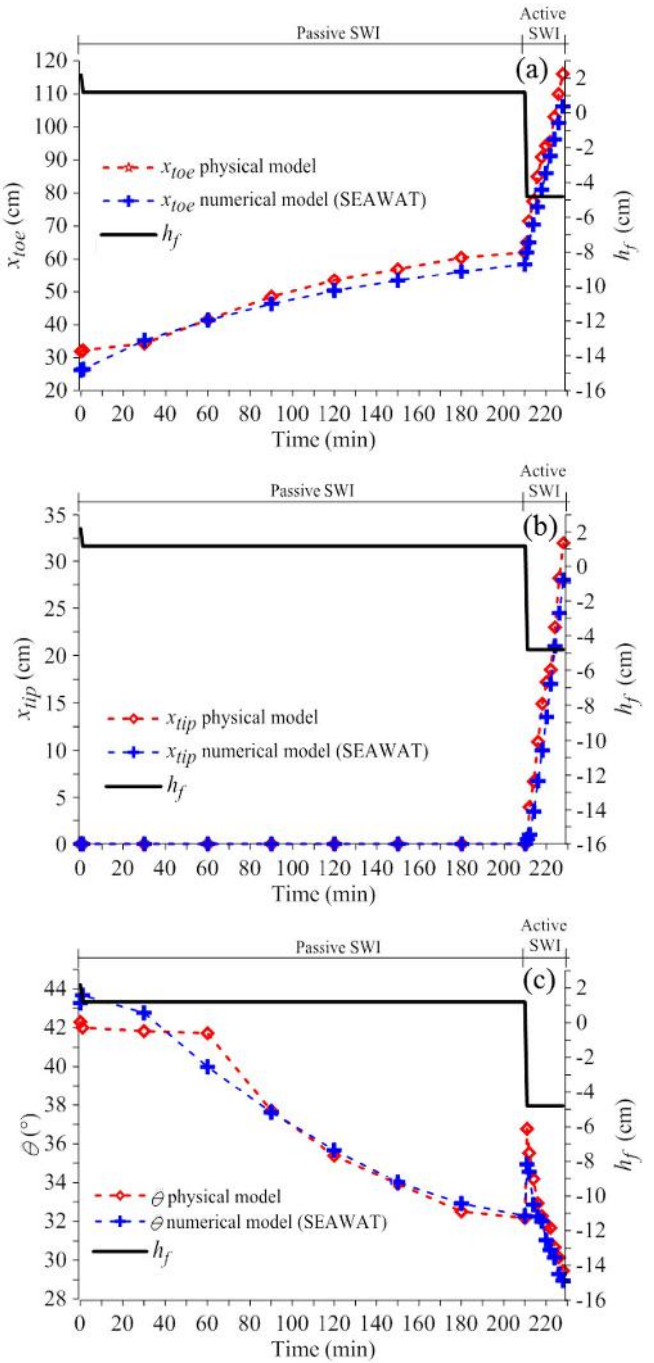


**Figure 4.** The temporal behavior of the freshwater-seawater interface under passive and active SWI at the laboratory scale, in terms of (a) wedge toe location, (b) wedge tip location, and (c) the interface alignment.

to explore the origins of WTS. Laboratory-scale results are shown in Figure 5 after 210 min of passive SWI (Figure 5a) and after 0.5 min of active SWI (Figure 5b). It can be seen that the saltwater circulation that was present under passive SWI (Figure 5a) ceased under active SWI (Figure 5b). WTS is clearly derived from the lateral movement of saltwater from the sea boundary.

### 4.2. Numerical Simulation of SWI Case Studies

The case studies of modified coastal aquifers include both active and passive SWI situations. The post-SWI $h_f$ values in Table 1 indicate that inland-sloping hydraulic gradients and active SWI have occurred in Cases 1, 3, and 4, whereas Case 2 has experienced a seaward-sloping hydraulic gradient and passive SWI conditions. Figure 6 shows the simulated position of the 5%, 50%, and 95% seawater salinities for the four case studies, following gradual FHDs at rates and magnitudes listed in Table 1. Significant WTS occurred in Cases 1, 3, and 4. $x_{tip}$ values for Cases 1 and 3 were 597 and 415 m, respectively. In Case 4, $x_{toe}$ reached the inland boundary (at 2700 m) after 24 years of FHD, which was prior to the completion of the 39 years simulation period. Therefore, an earlier simulation time (i.e., 22 years) is presented in Figure 6 for Case 4 to avoid the inland boundary effect on the freshwater-saltwater interface. $x_{tip}$ in Case 4 was 542 m after 22 years. There was minor WTS in Case 2, in which the water table salinity exceeded 5% of seawater up to 18.4 m from the seaward boundary.

At the end of the simulation periods, $O_f$ was zero in all cases (i.e., the 5% seawater salinity had reached the water table), including the passive SWI case where dispersive processes led to brackish groundwater discharge to the sea. This result suggests that WTS could theoretically occur in field-scale coastal aquifers under both passive and active SWI situations. At the cessation of simulations, $\theta$ values for Cases 1, 2, 3, and 4 (i.e., after 22 years) were 2.9°, 4.9°, 9.6°, and 3.4°, respectively. In general, the values of $\theta$ obtained in the field-scale models are much less than the laboratory-scale model (see Figure 4c). This is

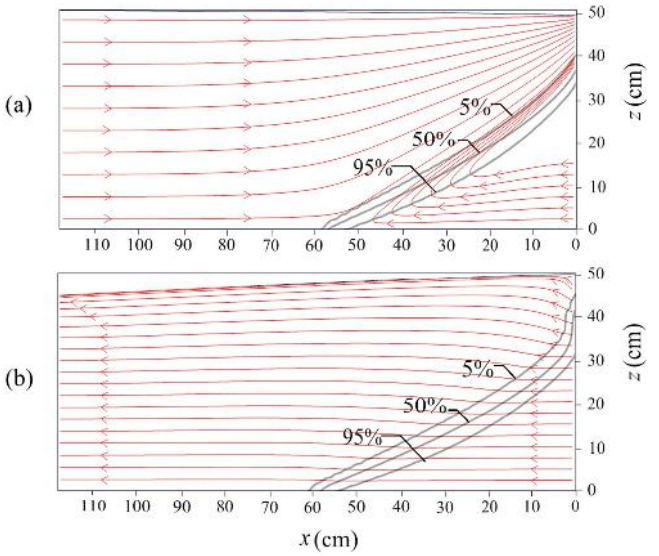


**Figure 5.** The results of particle tracking for (a) passive SWI after 210 min and (b) active SWI after 0.5 min.

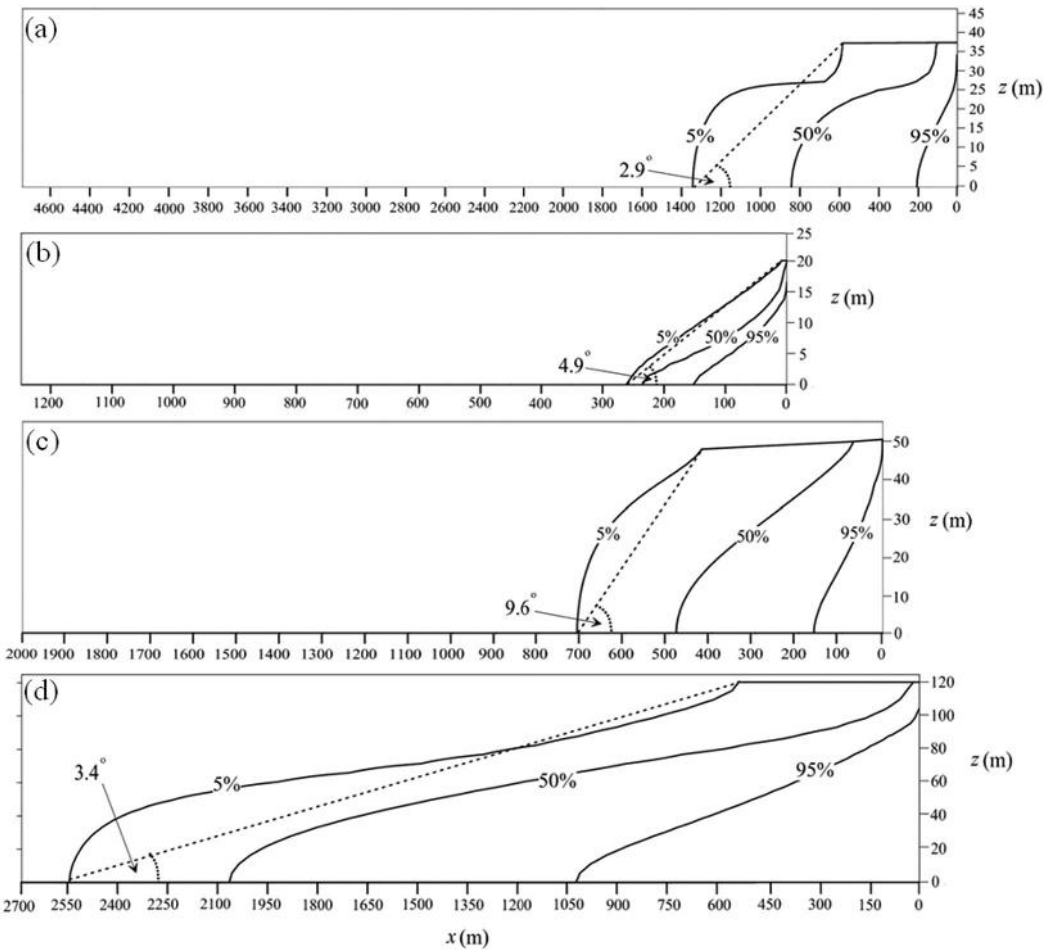


**Figure 6.** The results of SEAWAT numerical simulations after gradual inland FHD scenario for (a) Case 1, Pioneer Valley aquifer, (b) Case 2, Willunga Basin aquifer, (c) Case 3, Korba aquifer, and (d) Case 4, Exmouth aquifer (after 22 years).

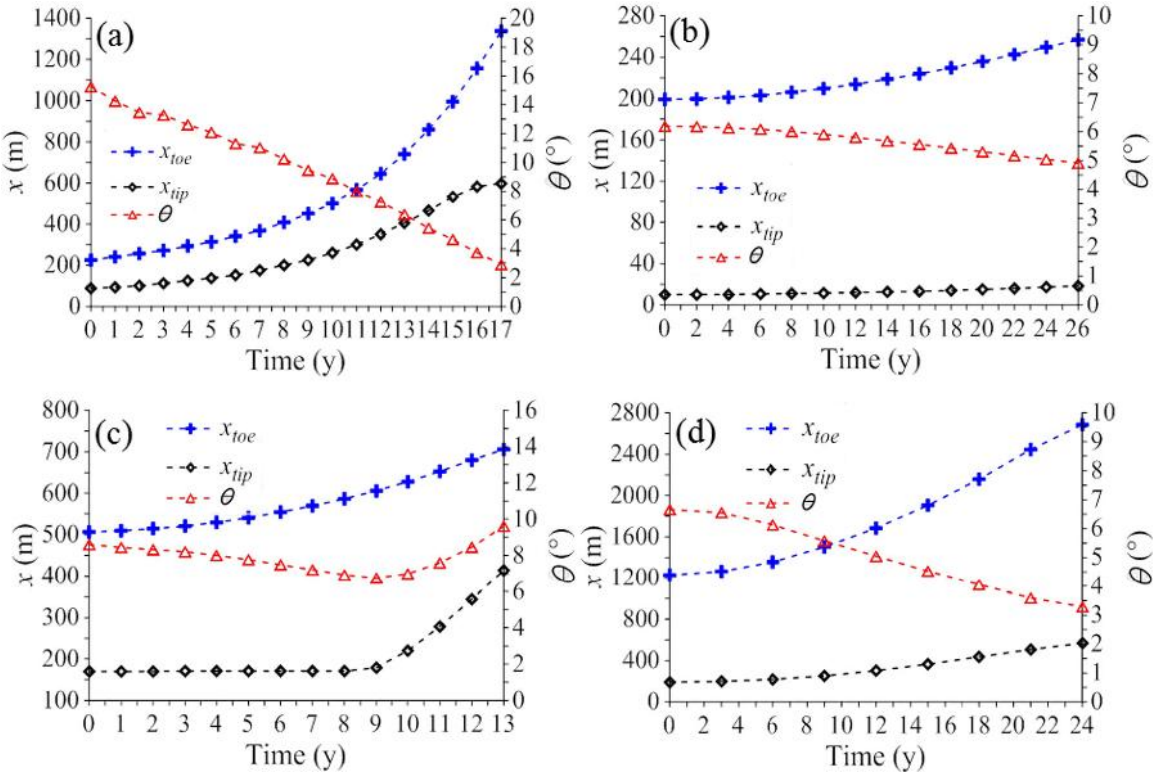


**Figure 7.** The freshwater-saltwater interface profile indicators for (a) Case 1, Pioneer Valley aquifer, (b) Case 2, Willunga Basin aquifer, (c) Case 3, Korba aquifer, and (d) Case 4, Exmouth aquifer.

attributable to the larger aspect ratio (i.e., the ratio of aquifer length to thickness) within the field-scale models (ranging from 22 to 128) relative to the laboratory-scale model (2.4).

Salinities at the water table (i.e., between the tip and coast) are predominantly less than 50% of seawater in all cases, indicating that WTS is primarily associated with brackish water from the mixing zone. Hence, longitudinal and transverse dispersivities, which control the width of the mixing zone [*Abarca et al.*, 2007], are critical aspects of WTS extent.

Temporal patterns in SWI are given in Figure 7, which shows continuous decreases in $\theta$ (i.e., the toe moved faster than the tip) with time in Cases 1, 2, and 4. In Case 3, $\theta$ decreased for the first 9 years and then increased for the remaining simulation period. This indicates that the movement of the interface tip became faster than the movement of the interface toe after 9 years. This lag in the response of the interface tip may be attributed to the relatively low $K$ used in Case 3 (i.e., $K$ is 7 m/d). That is, longer response times occur in aquifer systems characterized by lower $K$ values [*Watson et al.*, 2010]. A lag in the reduction of freshwater flux $q_0$ at the sea boundary was observed for Case 3, with $q_0$ reducing slowly from 0.46 to 0.06 $m^2$/d during the first 9 years. This phenomenon was not observed in Case 2 (i.e., $K$ is 10 m/d), which involved passive SWI, where changes in $q_0$ are more subdued (i.e., $q_0$ was 0.20 $m^2$/d at the end of the simulation period).

In order to explore the role of various parameters in controlling WTS, a sensitivity analysis was conducted using Case 4 as a base case. Different rates of FHD (0.18, 0.24 m/yr, instantaneous), $K$ (22.5, 67.5, 90.0, and 112.5 m/d), $\alpha_L$ (1, 20, 30, and 40 m), and $h_s$ (115 and 126 m) were used. The results presented in Figure 8 indicate that the magnitude of WTS is largest under conditions of high rates of FHD (Figure 8a), high $K$ (Figure 8b), high $\alpha_L$ (Figure 8c), and large $h_s$ (Figure 8d). It is shown in Figure 8d that a higher value of aquifer thickness $h_s$ may lead to an increase in SWI and WTS in coastal aquifers, even though the boundary head difference between the inland and coastal boundary remained the same. This is likely due to the change in the model's aspect ratio (the ratio of aquifer length to thickness), whereby decreasing this ratio (due to the increase of $h_s$) enhances SWI and therefore WTS. This is in agreement with the result of *Werner and Simmons* [2009] and *Lu and Werner* [2013] who showed that the extent of SWI is larger in a thicker

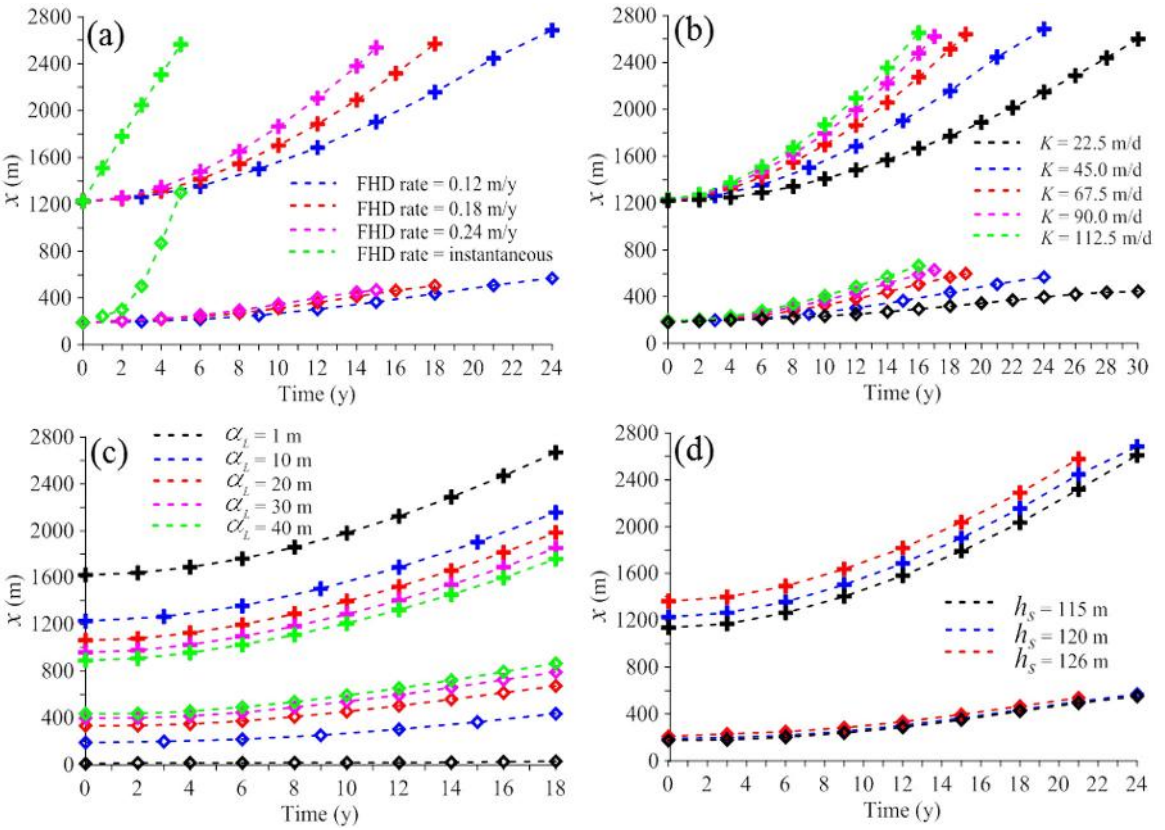


**Figure 8.** Sensitivity analysis for different values of (a) FHD rate, (b) hydraulic conductivity, (c) dispersivity, and (d) aquifer thickness, using Case 4 Exmouth aquifer as a base case. $x_{toe}$ trends are indicated by crosses (+) and $x_{tip}$ trends by diamonds (◇).

coastal aquifer, in response to the same boundary head differences. Interestingly, $x_{tip}$ increased and $x_{toe}$ decreased with higher values of $\alpha_L$ (Figure 8c). That is, higher dispersivity led to a smaller magnitude of SWI extent within the lower domain of the coastal aquifer than in the upper domain. This agrees with the results of *Kerrou and Renard* [2010], who showed that an increase in dispersion (i.e., due to a larger dispersivity parameter or heterogeneity) may cause a decrease in density contrast within the mixing zone and a larger zone of mixing. They concluded that this condition may lead to a rotation of the saltwater wedge, where its base will move seaward relative to the upper part.

## 5. Conclusions

SWI in unconfined coastal aquifers can result in WTS, which may induce soil salinization through capillary rise. There is presently limited guidance on the extent to which WTS may occur as a secondary impact of SWI. In this study, physical experiments and numerical modeling were used to explore WTS associated with SWI in various nontidal, unconfined coastal aquifer settings.

Laboratory experiments and corresponding numerical simulations show that significant WTS may occur under active SWI due to the associated cessation of fresh groundwater flow to the coast. Under passive SWI conditions, minor WTS might occur under certain conditions (i.e., high $\alpha_L$, high $K$, and low $q_0$) and as a result of dispersive processes, where the water table may exceed 5% of seawater salinity in the vicinity of the sea boundary.

Numerical modeling of published field cases shows that WTS may occur at rates of up to 60 m/yr, although supportive field evidence is presently lacking. Minor WTS was simulated in the Willunga Basin aquifer that is presently undergoing passive SWI, while major WTS was modeled in the other three published field cases (i.e., Pioneer Valley, Korba, and Exmouth aquifer) that have experienced active SWI. WTS during active SWI is larger for cases with higher $K$, rapid FHD, higher dispersivity parameters, and a thicker aquifer. These results

suggest that the likelihood of WTS in real-world settings is high under active SWI conditions, and hence further field substantiation and an evaluation of the implications for unsaturated zone salinization is needed, particularly within aquifers where groundwater levels have fallen below sea level.

**Acknowledgments**
Data used in this article are available by request addressed to the corresponding author. This research is a part of the PhD thesis of the first author at Flinders University. We thank Vincent Post, Craig Simmons, Sadjad Mehdizadeh, and Danica Jakovovic for helpful discussions regarding laboratory apparatus and SEAWAT modeling. We gratefully acknowledge the suggestions of three anonymous reviewers.

## References

Abarca, E., J. Carrera, R. Held, X. Sanchez-Vila, M. Dentz, W. Kinzelbach, and E. Vazquez-Sune (2004), Effective dispersion in seawater intrusion through heterogeneous aquifers, paper presented at 18th Salt Water Intrusion Meeting, Inst. of Geol. and Miner. Explor., Cartagena, Spain.

Abarca, E., J. Carrera, X. Sánchez-Vila, and M. Dentz (2007), Anisotropic dispersive Henry problem, *Adv. Water Res.*, *30*, 913–926, doi:10.1016/j.advwatres.2006.08.005.

Ayni, F. E., S. Cherif, A. Jrad, and M. Trabelsi-Ayadi (2011), Impact of treated wastewater reuse on agriculture and aquifer recharge in a coastal area: Korba case study, *Water Resour. Manage.*, *25*, 2251–2265, doi:10.1007/s11269-011-9805-2.

Bakker, M. (2006), Analytic solutions for interface flow in combined confined and semi-confined, coastal aquifers, *Adv. Water Res.*, *29*, 417–425, doi:10.1016/j.advwatres.2005.05.009.

Bear, J. (1979), *Hydraulics of Groundwater*, McGraw-Hill, N. Y.

Bear, J., and G. Dagan (1964), Moving interface in coastal aquifers, *J. Hydraul. Div.*, *90*, 193–216.

Benson, D. A., A. E. Carey, and S. W. Wheatcraft (1998), Numerical advective flux in highly variable velocity fields exemplified by saltwater intrusion, *J. Contam. Hydrol.*, *34*, 207–233, doi:10.1016/S0169-7722(98)00093-X.

Brovelli, A., X. Mao, and D. A. Barry (2007), Numerical modeling of tidal influence on density-dependent contaminant transport, *Water Resour. Res.*, *43*, W10426, doi:10.1029/2006WR005173.

Chiang, W. H., and W. Kinzelbach (1994), *PMPATH, An Advective Transport Model for Processing Modflow and Modflow*, Geol. Surv. of Hamb., Hamburg, Germany.

Cook, S., P. Dixon-Jain, M. Hocking, B. Sundaram, L. K. Morgan, K. M. Ivkovic, A. D. Werner, R. Norman, L. Caruana, and N. Garlapati (2013), A national-scale vulnerability assessment of SWI intrusion: Vulnerability factor analysis, *Rec. 2013/08*, Geosci. Austr., Canberra and Natl. Cent. for Groundwater Res. and Training, Adelaide, Australia.

Ferguson, G., and T. Gleeson (2012), Vulnerability of coastal aquifers to groundwater use and climate change, *Nat. Clim. Change*, *2*, 342–345, doi:10.1038/nclimate1413.

Fetter, C. W. (2001), *Applied Hydrogeology*, 4th ed., 598 pp., Prentice Hall, Upper Saddle River, N. J.

Freeze, A. R., and J. A. Cherry (1979), *Groundwater*, Prentice Hall, Englewood Cliffs, N. J.

Goswami, R. R., and T. P. Clement (2007), Laboratory-scale investigation of saltwater intrusion dynamics, *Water Resour. Res.*, *43*, W04418, doi:10.1029/2006WR005151.

Guo, W., and C. D. Langevin (2002), User's guide to SEAWAT: A computer program for simulation of three-dimensional variable-density groundwater flow, *U.S. Geol. Surv. Tech. Water Resour. Invest.*, Book 6, Chap. A7, 77 pp.

Ibrahimi, M. K., T. Miyazaki, T. Nishimura, and H. Imoto (2014), Contribution of shallow groundwater rapid fluctuation to soil salinization under arid and semiarid climate, *Arab. J. Geosci.*, *7*, 3901–3911, doi:10.1007/s12517-013-1084-1.

Intergovernmental Panel on Climate Change (2008), Climate change and water, *IPCC Tech. Pap. VI*, 210 pp., Geneva. [Available at http://www.ipcc.ch/.]

Jakovovic, D., A. D. Werner, and C. T. Simmons (2011), Numerical modelling of saltwater up-coning: Comparison with experimental laboratory observations. *J. Hydrol.*, *402*, 261–273, doi:10.1016/j.jhydrol.2011.03.021.

Jakovovic, D., V. E. A. Post, A. D. Werner, O. Männicke, J. L. Hutson, and C. T. Simmons (2012), Tracer adsorption in sand-tank experiments of saltwater up-coning, *J. Hydrol.*, *414*, 476–481, doi:10.1016/j.jhydrol.2011.11.024.

Johnson, A. I. (1967), Specific yield: Compilation of specific yields for various materials, *U.S. Geol. Surv. Open File Rep., 1662-D*, 119 pp. [Available at http://pubs.usgs.gov/wsp/1662d/.]

Kerrou, J., and P. Renard (2010), A numerical analysis of dimensionality and heterogeneity effects on advective dispersive seawater intrusion processes, *Hydrogeol. J.*, *18*, 55–72, doi:10.1007/s10040-009-0533-0.

Klute, A., and C. Dirksen (1986), Hydraulic conductivity and diffusivity: Laboratory methods, in *Methods of Soil Analysis, Part 1, Physical and Mineralogical Methods, Agronomy Monograph*, vol. 9, 2nd ed., pp. 687–734, Am. Soc. of Agron. and Soil Sci. Soc. of Am., Madison, Wis.

Kouzana, L., A. B. Mammou, and M. S. Felfoul (2009), Seawater intrusion and associated processes: Case of the Korba aquifer (Cap-Bon, Tunisia), *C. R. Geosci.*, *341*, 21–35, doi:10.1016/j.crte.2008.09.008.

Langevin, C. D., W. B. Shoemaker, and W. Guo (2003), MODFLOW-2000, The US Geological Survey modular ground-water model-documentation of the SEAWAT-2000 version with the variable-density flow process (VDF) and the integrated MT3DMS transport process (IMT), *U.S. Geol. Surv. Open File Rep.*, *03-426*.

Langevin, C. D., D. T. Thorne Jr., A. M. Dausman, M. C. Sukop, and W. Guo (2008), SEAWAT version 4: A computer program for simulation of multi-species solute and heat transport, *U.S. Geol. Surv. Tech. Methods, Book 6, Chap. A22*, 39 pp.

Lu, C., and A. D. Werner (2013), Timescales of seawater intrusion and retreat, *Adv. Water Res.*, *59*, 39–51, doi:10.1016/j.advwatres.2013.05.005.

Mahesha, A. (1995), Parametric studies on the advancing interface in coastal aquifers due to linear variation of the freshwater level, *Water Resour. Res.*, *31*, 2437–2442, doi:10.1029/95WR02040.

Mehdizadeh, S. S., A. D. Werner, F. Vafaie, and S. Badaruddin (2014), Vertical leakage in sharp-interface seawater intrusion models of layered coastal aquifers, *J. Hydrol.*, *519*, 1097–1107, doi:10.1016/j.jhydrol.2014.08.027.

Morgan, L. K., A. D. Werner, and C. T. Simmons (2012), On the interpretation of coastal aquifer water level trends and water balances: A precautionary note, *J. Hydrol.*, *470*, 280–288, doi:10.1016/j.jhydrol.2012.09.001.

Morgan, L. K., A. D. Werner, K. M. Ivkovic, H. Carey, and B. Sundaram (2013a), A national-scale vulnerability assessment of seawater intrusion: First-order assessment of seawater intrusion for Australian case study sites, *Rec. 2013/19*, Geosci. Aust., Canberra and Natl. Cent. for Groundwater Res. and Training, Adelaide, Australia.

Morgan, L. K., A. D. Werner, M. J. Morris, and M. D. Teubner (2013b), Application of a rapid-assessment method of SWI: Willunga Basin, South Australia, in *Groundwater in the Coastal Zones of Asia-Pasific*, vol. 7, pp. 1–30, edited by C. Wetzelhuetter, Springer, Dordrecht, doi:10.1007/978-94-007-5648-9_10.

Morgan, L. K., L. Stoeckl, A. D. Werner, and V. E. Post (2013c), An assessment of seawater intrusion overshoot using physical and numerical modeling, *Water Resour. Res.*, *49*, 6522–6526, doi:10.1002/wrcr.20526.

Ogata, A., and R. B. Banks (1961), A solution of the differential equation of longitudinal dispersion in porous media, *U.S. Geol. Surv. Prof. Pap.*, *411-A*, 7 pp. [Available at http://pubs.er.usgs.gov/publication/pp411A/.]

Ojuri, O., and S. Ola (2010), Estimation of contaminant transport parameters for a tropical sand in a sand tank model, *Int. J. Environ. Sci. Technol.*, *7*, 385–394, doi:10.1007/BF03326148.

Prathapar, S. A., C. W. Robbins, W. S. Meyer, and N. Jayawardane (1992), Models for estimating capillary rise in a heavy clay soil with a saline shallow water table, *Irrig. Sci.*, *13*, 1–7, doi:10.1007/BF00190238.

Schincariol, R. A., and F. W. Schwartz (1990), An experimental investigation of variable density flow and mixing in homogeneous and heterogeneous media, *Water Resour. Res.*, *26*, 2317–2329, doi:10.1029/WR026i010p02317.

Shi, L., L. Cui, N. Park, and P. S. Huyakorn (2011), Applicability of a sharp-interface model for estimating steady-state salinity at pumping wells-validation against sand tank experiment, *J. Contam. Hydrol.*, *124*, 35–42, doi:10.1016/j.jconhyd.2011.01.005.

Voss, C. I., and W. R. Souza (1987), Variable density flow and solute transport simulation of regional aquifers containing a narrow freshwater-saltwater transition zone, *Water Resour. Res.*, *23*, 1851–1866, doi:10.1029/WR023i010p01851.

Watson, T. A., A. D. Werner, and C. T. Simmons (2010), Transience of seawater intrusion in response to sea level rise, *Water Resour. Res.*, *46*, W12533, doi:10.1029/2010WR009564.

Werner, A. D., and M. R. Gallagher (2006), Characterisation of sea-water intrusion in the Pioneer Valley, Australia using hydrochemistry and three-dimensional numerical modelling, *Hydrogeol. J.*, *14*, 1452–1469, doi:10.1007/s10040-006-0059-7.

Werner, A. D., and D. A. Lockington (2004), The potential for soil salinization above aquifers impacted by seawater intrusion, in *Proceedings of 13th International Soil Conservation Organisation Conference: Conserving Soil and Water for Society: Sharing Solutions*, edited by S. R. Raine et al., 6 pp., ASSSI/IECA, Brisbane.

Werner, A. D., and D. A. Lockington (2006), Tidal impacts on riparian salinities near estuaries, *J. Hydrol.*, *328*, 511–522, doi:10.1016/j.jhydrol.2005.12.011.

Werner, A. D., and C. T. Simmons (2009), Impact of sea-level rise on sea water intrusion in coastal aquifers, *Ground Water*, *47*, 197–204, doi:10.1111/j.1745-6584.2008.00535.x.

Werner, A. D., D. Jakovovic, and C. T. Simmons (2009), Experimental observations of saltwater up-coning, *J. Hydrol.*, *373*, 230–241, doi:10.1016/j.jhydrol.2009.05.004.

Werner, A. D., J. D. Ward, L. K. Morgan, C. T. Simmons, N. I. Robinson, and M. D. Teubner (2012), Vulnerability indicators of sea water intrusion, *Ground Water*, *50*, 48–58, doi:10.1111/j.1745-6584.2011.00817.x.

Werner, A. D., Q. Zhang, L. Xue, B. D. Smerdon, X. Li, X. Zhu, L. Yu, and L. Li (2013), An initial inventory and indexation of groundwater mega-depletion cases, *Water Resour. Manage.*, *27*, 507–533, doi:10.1007/s11269-012-0199-6.